Abnormal autophagy is a critical mechanism in TANGO2-related rhabdomyolysis

Sebastian Montealegre[1≠], Hortense de Calbiac[1,2≠*], Marjolène Straube[1,2], Hugo Debruge[1,2], Loïc Chentout[1,2], Sorana Ciura[3], Apolline Imbard[4], Edouard Le Guillou[4], Anca Marian[3], Nicolas Goudin[5], Laure Caccavelli[1,2], Sylvie Fabrega[6], Arnaud Hubas[7], Peter van Endert[1,8], Nicolas Dupont[1], Julien Diana[1], Edor Kabashi[3≠], Pascale de Lonlay[1,2≠]

≠ equal contribution

[1]Université Paris Cité, INSERM, CNRS, Institut Necker Enfants Malades, F-75015 Paris, France

[2]Reference Center of Inherited Metabolic Diseases, Hôpital Universitaire Necker-Enfants Malades,, AP-HP, Institut Imagine, Filière G2M, MetabERN, F-75015, Paris, France

[3]Translational Research for Neurological Diseases, Institut Imagine, INSERM UMR 1163, Université Paris Cité, F-75015, Paris, France

[4]Metabolic biochemistry, Hôpital Universitaire Necker-Enfants Malades, AP-HP, Institut Imagine, Filière G2M, MetabERN, Université Paris Cité, F-75015, Paris, France

[5]Cell Imaging & Flow Cytometry Core Facilities, Structure Fédérative de Recherche Necker, INSERM US24/CNRS UMS3633, F-75015, France

[6]Platform, Structure Fédérative de Recherche Necker, F-75015, Paris, France

[7]Genetics and Molecular Biology, Laboratoire de culture cellulaire, Hôpital Universitaire Cochin, AP-HP, F-75014, Paris, France

[8]Service Immunologie Biologique, AP-HP, Hôpital Universitaire Necker-Enfants Malades, F-75015, Paris, France

*__Corresponding author :__ Dr Hortense de Calbiac

Inserm U1151, Institut Necker Enfants-Malades, 160 rue de Vaugirard, Paris France

Telephone number: 00 33 6 19 46 23 36

E-mail address: hortense.de-calbiac@institutimagine.org

Abstract

Patients with pathogenic variants in the TANGO2 gene suffer from severe and recurrent rhabdomyolysis (RM) episodes precipitated by fasting. Since starvation promotes autophagy induction, we wondered whether TANGO2-related muscle symptoms result from autophagy insufficiency to meet cellular demands in stress conditions. Autophagy functioning was analyzed in vitro, in primary skeletal muscle cells from TANGO2 patients in basal and fasting conditions. In addition, wce developed a tango2 morphant zebrafish model to assess the effect of tango2 knockdown (KD) on locomotor function and autophagy efficiency in vivo. We report that TANGO2 mutations are associated with decreased LC3-II levels upon starvation in primary muscle cells, but not in fibroblasts. In zebrafish larvae, tango2 knockdown induces locomotor defects characterized by reduced evoked movements which are exacerbated by exposure to atorvastatin, a compound known to cause RM. Importantly, RM features of tango2 KD are also associated with autophagy defects in zebrafish. Calpeptin treatment, a known activator of autophagy, is sufficient to rescue the locomotor function and improves autophagy in zebrafish. LC3-II levels of primary muscle cells of TANGO2 patients are also ameliorated by calpeptin treatment. Overall, we demonstrate that TANGO2 plays an important role in autophagy, and that autophagy efficiency is critical to prevent RM, thus giving rise to new therapeutic perspectives in the prevention of these life-threatening episodes in the context of TANGO2 pathology.

Keywords: autophagy; calpeptin; myoblasts; rhabdomyolysis**;** TANGO2; zebrafish

Abbreviations

ATV: atorvastatin; dpf: days post-fertilization; ER: endoplasmic reticulum; hpf: hours post-fertilization; KD: knockdown; KO: knockout; LC3: Microtubule-associated protein 1A/1B light chain 3B; MO: morpholino; RM: rhabdomyolysis; TANGO2: Transport and Golgi Organization Protein 2 Homolog

Introduction

Transport and Golgi Organization Protein 2 Homolog (TANGO2)-related disease is a pathology with a poor prognosis due to the recurrence of severe life-threatening rhabdomyolysis (RM) bouts [1, 2], characterized by the acute breakdown of skeletal myofibers [3, 4]. Other symptoms of TANGO2 disease are developmental regression, hypoglycemia, hypothyroidism and cardiac arrhythmia, including prolonged QTc interval or ventricular fibrillation [1, 2, 5-12]. RM can be triggered by fasting and infections, but also by exposure to cold or heat. TANGO2 function is poorly understood but has been reported to be required for endoplasmic reticulum (ER) - Golgi [1, 12-15], and haem [16] transports. Depletion of TANGO2 results in slowed cargo movements between the ER and the Golgi in patient's fibroblasts [14], ER and Golgi fusion in Drosophila cells [13], and/or abnormal ER/Golgi morphology in different models [1, 12, 14-16]. However, abnormal ER morphology in patients' cells has not been systematically observed [1, 5]. On the other hand, besides the vicinity of the ER [12, 15], TANGO2 is mainly cytosolic [7] where it has been shown to partially localize to mitochondria [2, 9, 14, 17, 18] and lipid droplets [19]. Importantly, the overall abundance of major membrane and cellular lipids synthesized through ER/sarcoplasmic reticulum is significantly decreased in *tango2* mutant zebrafish at the basal level in the absence of any external trigger [15], and in Hep2g cells [19]. Plasma and fibroblasts from TANGO2 patients exhibit abnormal accumulation of fatty acids and/or a defect in palmitate-dependent oxygen consumption suggesting impairment in mitochondrial fatty acid oxidation [2, 9, 12, 17]. However, we previously showed that the main mitochondrial functions, including respiratory chain, fatty acid beta-oxidation, and Krebs cycle were normal in primary myoblasts from TANGO2 patients, implying that mitochondrial defects could be a secondary effect, with the pathogenic RM trigger remaining unknown [5]. In a therapeutic perspective, it has recently been reported that panthotenic acid (Vitamin B5) can rescue the defects of ER to Golgi transport in TANGO2 knockout (KO) fibroblasts [13], as well as several behavioural traits of *tango2* knockdown (KD) Drosophila [13] and patients [11, 20].

Interestingly, TANGO2 patients exhibit normal muscle function between RM episodes, suggesting that muscle metabolism is sufficient to meet cellular demands except in stress conditions. Starvation being a well-known activator of autophagy, we hypothesized that autophagy insufficiency is a critical event in RM triggering that needs to be targeted and restored to prevent these life-threatening episodes. To address this hypothesis, we examined autophagy flux in TANGO2 patients' cells and report a defect in Microtubule-associated protein 1A/1B light chain 3B (hereafter referred to as LC3) levels upon starvation, in primary muscle cells from patients. We translated our observation from patients' cells to *tango2* knockdown (KD) zebrafish that reproduces motor defects under basal conditions, as recently described [15, 16], or through addition in this vertebrate model of atorvastatin, a compound well known to induce RM. We found that *tango2* KD zebrafish display abnormal autophagy and that calpeptin treatment rescues the associated locomotor phenotype *in vivo*, as well as autophagy function both *in vivo* and *in vitro*, thus raising new therapeutic perspectives for TANGO2-related RM.

Results

TANGO2 plays a role at the initiation of autophagy in primary myoblasts.

To determine whether TANGO2 plays a role in autophagy, we incubated primary myoblasts either in growth medium (GM) or in starvation medium (EBSS) for various durations, in the presence or absence of bafilomycin A, an inhibitor of autophagosome and lysosome fusion. Remarkably, we found a significant reduction of LC3-II absolute levels upon starvation in cells of three patients relative to three controls in at least two technical replicates per patient (**Fig. 1A and B**). This decrease in LC3-II levels could be partially rescued by bafilomycin A, indicating that patient autophagosomes can fuse with lysosomes, although at a lower rate than control cells. Further validating these results, LC3-II levels were decreased upon siRNA-mediated *TANGO2* KD in control myoblasts (**Fig. 1C**). Reduction of LC3 transcript expression upon starvation was also confirmed by qPCR in patient's myoblasts, as compared to the controls (**Fig. 1D**).

Furthermore, we found that LC3-II levels were normal in TANGO2 fibroblasts, whereas these parameters were significantly reduced in myoblasts from the same patients, indicating potential tissue specificity for the requirement of TANGO2 in the initiation of autophagy (**Fig. 1E**). Prompted by the observation that starvation-induced autophagy is defective in patient's myoblasts, we tested whether other forms of autophagy would be defective as well. Basal autophagy was measured by quantification of LC3-II levels over time in the presence of bafilomycin A and showed interpatient variability condition, as opposed to starvation-induced autophagy (**Fig. S1A and B**)..

Since the absence of TANGO2 leads to defective autophagy, we asked whether TANGO2 WT colocalizes with LC3-II autophagosomes. Using lentiviral expression of FLAG-tagged plasmids expressing WT TANGO2 or a mutant reported in patients [1] (Glycine154Arginine, G2R) and immunolabelling, we failed to detect TANGO2 in the vicinity of autophagosomes upon starvation

(**Fig. 1F)**. Instead, we found that the vast majority of TANGO2 resides in the cytosol (**Fig. S1A**), in agreement with previous observations [7], and co-localizes little with the mitochondrial marker TOM20 (**Fig. S1C**, cell 1) in partial agreement with previous data showing a mitochondrial localization and function of TANGO2 [1, 17]. Since TANGO2 has been reported by others to play a role in mitochondria [2, 9, 14, 17], we further examined transduced cells to detect any partial localization of TANGO2 to mitochondria. Indeed, in a small subset of cells, TANGO2 WT partially localized to mitochondria (**Fig. S1C**, cell 2 and right inset). Moreover, the TANGO2 G2R Cter-FLAG mutant is present at mitochondrial vesicles (**Fig. S1C**). In contrast, the two TANGO2 variants with an N-terminal domain FLAG tag showed a cytosolic localization and were mostly excluded from mitochondria, irrespective of the G2R mutation (**Fig. S1C**). These data indicate that the reported mitochondrial localization of TANGO2 requires its N-terminal domain as well as unperturbed Glycine 154. Examining the expression of our constructs by Western Blotting, we noticed the presence of a band between 100-130 kDa that seems to be present only in the WT – Cter version of TANGO2 (**Fig. S1D and E**). Both FLAG and TANGO2 Proteintech antibodies can detect this band, which is not the case for lower molecular weight bands. These data suggest that TANGO2 can exist as an oligomer resistant to SDS and reducing agent, depending on the availability of the N-terminal domain of the protein.

In agreement with the minor TANGO2 mitochondrial localization at the steady state, and our previous report on normal beta-oxidation flux in patient's myoblasts [5], we did not find any abnormalities of beta-oxidation flux [21] in whole blood of three TANGO2 patients compared to controls (**Table 1**).

Taken together, these data suggest that compromised autophagy mediated by TANGO2 in muscle cells plays a major pathogenic role, while in our hands, the mitochondrial function of TANGO2 described mostly in patient fibroblasts [9, 17], remains to be determined in muscle cells and in blood.

TANGO2 morphant zebrafish displays a RM-like locomotor phenotype due to autophagy defects

Zebrafish is a vertebrate organism widely used to model genetic conditions and major health disorders, including in the context of muscular [22-24] and autophagy-related diseases [25-27]. Zebrafish skeletal muscles spontaneously start to contract as soon as 17 hours post-fertilization (hpf). By 24 hpf, myotomes are present thus enabling the embryo to coil and even respond to touch. By 48 hpf, the muscle is fully differentiated and zebrafish larvae display stereotyped escape responses to touch, allowing for an assessment of muscle performance and function using the Touch-Evoked Escape Reponse (TEER) test. We confirmed by qPCR that a *TANGO2* orthologue is expressed in zebrafish at early development stages, at 1 and 2 days post-fertilization (dpf) (**Fig. 2A**). We designed two different antisense oligonucleotides coupled to the morpholino moiety (MOs) to down-regulate tango2 expression in zebrafish: tango2-MO^{atg} is predicted to sterically prevent tango2 translation by targeting its initial AUG codon, while tango2-MO^{spE3} is predicted to alter tango2 splicing by targeting exon3-intron3 junction. Noteworthy, this splicing induction resembles the large exon3-exon 9 deletion in humans. We did not observe any developmental deficit or non-specific toxicity in the different experimental conditions as illustrated by the results obtained at 50 hours post fertilization (hpf) (**Fig. 2B**). In zebrafish, the RM phenotype is defined by reduced locomotion parameters and/or disrupted muscle morphology [16, 28, 29]. Here, RM phenotype as evoked motor response was assessed through the TEER test to assess muscle performance, as previously described [30]. Individual swimming episodes were traced for zebrafish from control-MO, tango2-MO^{atg} and tango2-MO^{spE3} (**Fig. 2C**). We observed a decreased locomotion in tango2-MO^{spE3} condition, but not in tango2-MO^{atg} condition, as compared to controls (**Fig. 2C and D**). Quantitative analysis of the TEER demonstrated that tango2-MO^{spE3} induces a locomotor phenotype, as shown by significantly decreased distance (**Fig. 2D**), which is consistent with recent observations in CRISPR KO *tango2* models [15, 16]. We took advantage of the fact that

tango2-MO^{spE3} is predicted to affect tango2 expression at the RNA level, to validate *tango2* knockdown in this condition, at 1 and 2 dpf, by gel electrophoresis of the amplicon of the targeted region (**Fig. 2E**).

To validate the specificity of this locomotor phenotype, we exposed 30 hpf zebrafish to atorvastatin (ATV, Lipitor), usually employed for the treatment of hypercholesterolemia, and proceeded to TEER analysis at 50 hpf. Statin treatments are known to induce RM, in particular in the context of an underlying genetic predisposition [31] and ATV has previously been shown to induce RM in zebrafish [29]. TEER quantification demonstrated that ATV treatment exacerbates the locomotor defects of tango2-MO^{spE3} zebrafish, in a dose-dependent manner (**Fig. 2F**). Indeed, while at the highest dose of 1 μM ATV, zebrafish displayed decreased swimming properties in all conditions (**Fig. 2F**), incubation with 0.5 μM ATV led to motor deficits only upon *tango2* KD, in both tango2-MO^{spE3} and tango2-MO^{atg}, suggesting that another RM-specific stress is necessary to unveil RM phenotype in tango2-MOatg condition (**Fig. 2F**).

We wondered whether autophagy disruption correlates with a locomotor phenotype in *tango2* zebrafish morphants. To test this hypothesis, we used the GFP-LC3-RFP-LC3ΔG fluorescent probe [26]. Upon autophagy induction, the probe is cleaved, giving rise to ectopic expression of GFP-LC3 and RFP-tagged LC3ΔG mutant. GFP-LC3 is then integrated into the membrane of the autophagosome before degradation in the lysosome, whereas RFP-LC3ΔG remains in the cytosol. Thus, the autophagy index, as measured by GFP/RFP fluorescence ratio for 30 hpf zebrafish dissociated cells, inversely correlates with autophagy efficiency [26]. We observed that the autophagy index was significantly increased in tango2-MO^{spE3} zebrafish cells, when compared to controls, indicating compromised autophagy in this condition (**Fig. 2G and S2**). However, dissociated cells from tango2-MO^{atg} zebrafish showed no difference relative to controls, confirming that zebrafish locomotor properties correlate with autophagy efficiency.

Calpeptin treatment rescues TANGO2 pathology in vivo and in vitro

To counteract autophagy defects in tango2-MO^{spE3} zebrafish, we treated 30 hpf larvae with calpeptin, a calpain inhibitor known to activate autophagy including in zebrafish [32] and previously used as a potential therapeutic in a Machado-Joseph zebrafish model [33]. Calpeptin treatment was sufficient to normalize locomotor parameters of tango2-MO^{spE3} zebrafish, and increased the travelled distance in treated zebrafish significantly (**Fig. 3A**). Importantly, we observed that the autophagy flux of tango2-MO^{spE3} cells is also improved by calpeptin treatment (**Fig. 3B**). Having discovered that inducing autophagic flux in zebrafish by calpeptin treatment reverts the disease phenotype in tango2 deficient zebrafish, we tested whether calpeptin treatment can improve the defective LC3-II levels in primary TANGO2 patient myoblasts (**Fig. 3C and D**). Indeed, calpeptin restored LC3-II levels in primary TANGO2 KO myoblasts treated with EBSS starvation equivalently to those of untreated control cells (**Fig. 3C and D**). Even though autophagy index was not equivalent to calpeptin-treated control myoblasts, these results demonstrate that calpeptin treatment can improve autophagy efficiency in these cells.

Discussion

Here, we report that TANGO2 protein has a role in the regulation of autophagy. Indeed, we observed that TANGO2 deficiency results in reduced LC3-II levels upon starvation in primary muscle cells from patients, and in defective autophagy in zebrafish. Our observation that the starvation-induced autophagy does not show any alteration in skeletal fibroblasts from the same TANGO2 deficient patients indicates that the RM pleiotropy of TANGO2 pathology could be due to tissue-specificity of autophagy dysfunction in organs at risk of decompensation during fasting. Functional autophagy is essential for the maintenance and adaptation to stress of muscle cells, and defects in all steps of this pathway have been associated with skeletal muscle diseases [34-39],

including metabolic RM [40, 41]. Supporting that, *tango2* KD led to reduced evoked swimming parameters in zebrafish, which is consistent with recent studies showing a myopathy-like phenotype in zebrafish upon *tango2* knockout KO [15, 16]. We also show that incubation of *tango2* KD zebrafish with atorvastatin, a drug known to induce RM [31, 42] including in zebrafish [29, 43], exacerbates the motor deficits observed in *tango2* KD, thus confirming the specificity of *tango2* KD phenotype. Furthermore, we corroborate *in vivo* that the RM-like phenotype induced by *tango2* loss of function correlates with an impaired autophagy flux, as demonstrated by the decreased degradation of autophagosomes containing exogenous LC3. Importantly, we demonstrate that restoring autophagy function by calpeptin, a calpain inhibitor, is sufficient to rescue the RM-like phenotype in *tango2* KD zebrafish, as well as to improve LC3-II levels in starved TANGO2 primary myoblasts.

Recent advances in the understanding of TANGO2 disease point towards defects in lipid metabolism with decreased overall abundances of membrane and cellular lipids inducing defective anterograde ER-to-Golgi transport or defective haem export in cellular and animal models [13, 15, 16, 19]. Two recent preprints have shown abnormal lipid profiles in TANGO2 models, with reduced levels of phosphatidic acid and increased levels of its unacetylated precursor, lysophosphatidic acid, in Hep2g cells [19], and decreased phosphatidylcholine and triglycerides in zebrafish [15]. Considering that i) starvation affects lipid metabolism and autophagy, ii) membrane lipid composition is critically involved in autophagy regulation and processing [44], iii) the ER-ERGIC-Golgi axis provides membranes to form autophagosomes, thereby connecting vesicular forward transport with autophagy, iv) the reports on defective lipid metabolism in TANGO2 KO cells and animal models, and v) the autophagy defect in TANGO2 deficient models observed in this study, it is likely that TANGO2 is involved in the metabolism of lipids of membrane structures participating in autophagy and that TANGO2-related muscle symptoms are the consequence of insufficient autophagy in patients exposed to stress condition, such as starvation triggering

autophagy. In this sense, we and others have previously demonstrated that mutations in the phosphatidate phosphatase *LPIN1*, another genetic cause of RM predisposition, lead to a selective loss of phosphatidylinositol-3-phosphate [40, 45], which is particularly enriched in autophagosomes and involved in all steps of autophagy [46], with subsequent autophagy impairment [40, 45]. Abnormal phospholipids and autophagy defect have been also associated with other skeletal myopathies such as Vici syndrome [41]. Overall, this raises the hypothesis that mutations in genes involved in lipid metabolism can converge to autophagy insufficiency which can be exacerbated by stress conditions, such as starvation, thus leading to RM outbreak.

In physiological conditions, we observe that the vast majority of TANGO2 localizes to the cytosol and only a minor portion to mitochondria, in agreement with two previous reports [14, 16]. These observations are in line with our previous study, where we did not observe any anomalies in metabolic beta-oxidation flux in such cells upon palmitate loading, or in mitochondrial structure and function [5]. Consistently, the mitochondrial membrane decoupling by CPPP resulted in normal induction of autophagy in this study. This is in agreement with previous studies, which also found normal OXPHOS in patient's cells [7] or in TANGO2 iPSC derived cardiomyocytes [47]**.** Furthermore, despite abnormal acylcarnitine profiles in plasma of some patients [1, 2, 9, 12], we show a normal mitochondrial flux beta-oxidation in whole blood of TANGO2 deficient patients (**Table 1**). Consequently, the reported restoration of CoA by vitamin B5 [13, 20], the obligate precursor of CoA, an essential pathway conserved in both prokaryotes and eukaryotes, may concern cytosolic CoA, as the intramitochondrial coenzyme A pool is not limiting for the mitochondrial beta-oxidation pathway. A possible way to reconcile these observations made in different models would place TANGO2 as an important protein in the cytosol, notably as an intermediate in cytosolic CoA formation, thereby acting as an upstream membrane precursor to form COPII vesicles or autophagosomes. Interestingly, immunofluorescence experiments in primary myoblasts ruled out a direct TANGO2 localization to autophagosomes, including under starvation. Under nutrient-rich

conditions, constitutive ER to Golgi transport is already affected in TANGO2 KO cells by the constitutive nature of this process [14]. Conversely, basal autophagy was found abnormal in one patient and normal in another, suggesting that the distinct severity of TANGO2 patients' symptoms may rely on differentially affected autophagy under steady state.

Apart from the defect in autophagy found in patient myoblasts and zebrafish, we found that overexpressed TANGO2 G154R -FLAG mutant [1] in myoblasts localizes more prominently to mitochondria than its WT counterpart. On the basis of these observations, we speculate that TANGO2 can be constitutively recruited to mitochondria via its mitochondrial localization signal at the N-terminus [14] and cycle back to the cytosol. The mutation G154R might act as an anchor to a mitochondrial protein, preventing its release to the cytosol. Finally, recent work has reported that TANGO2-GFP is expressed at the expected size in various cell lines [14, 19]. Our observation of a band between 100-130 kDa detectable upon prolonged exposure in control but not patient cells might indicate that TANGO2 can oligomerize, although at a very minor rate. Further biochemical studies, as well as the development of antibodies against TANGO2 that work in immunofluorescence staining would be instrumental for studying this hypothesis.

In conclusion, our results support that abnormal autophagy is a critical mechanism in TANGO2-related RM pathophysiology that needs to be targeted in a therapeutic perspective. In addition, we report the autophagy activator calpeptin as a candidate for prevention of RM bouts in TANGO2 patients.

Methods

Patient myoblasts. Myoblasts from three patients were obtained from skeletal muscle biopsy from individuals (deltoid region) and 3 age-matched control individuals (paravertebral region). Human primary myoblasts were isolated and grown as described [40]. The patients harbored pathogenic variants in *TANGO2* gene (Patient 1 and Patient 3: homozygous deletion Exon 3-Exon 9, Patient 2: homozygous c.262C>T (p.Arg88) found by next generation sequencing (NGS) [5]. Informed consent was obtained from TANGO2 patients and controls after obtaining the ethics approval to work on human samples by the *Comité pour la protection des personnes* (CPP, 2016) and the declaration of human myoblasts to the *Département de la Recherche Clinique et du Développement*.

Plasmids, lentivirus production, and transduction. Codon optimized 2X FLAG TANGO2 WT (NP_001270035) was inserted into pMK-T or pLVX-EF1α-IRES-puro with restriction sites SpeI/NotI by GeneArt (Thermosfisher, Germany). The mutant 2X FLAG TANGO2 Gly154Arg was generated with the In-Fusion HD Cloning Plus Kit (Takara Bio Europe) following the manufacturer's instructions using the pMK-T plasmid as template, and then cloned into pLVX-EF1α-IRES-puro, to produce pLVX 2X FLAG TANGO2 G2R. To generate C-terminal fusion proteins, the FLAG tag was removed as above, serving as a template to generate pMK-T TANGO2 WT-2X FLAG C-ter or pMK-T TANGO2 G2R-2X FLAG C-ter. Subsequently, the inserts were cloned into pLVX-EF1α-IRES-puro to produce pLVX TANGO2 WT-2X FLAG Cter or pLVX TANGO2 G2R-2X FLAG Cter. Plasmid DNA was extracted and purified with Nucleobond Xtra Maxi EF kit (Macherey- Nagel) and used to produce lentiviruses with an average titer of 10^9 TU/ml. Primary myoblasts at early passages were transduced at a MOI=50 in the presence of polybrene at 8 µg/ml, overnight. Next day, the medium was changed, and two days later, puromycin was added at a final concentration of 5 µg/ml. Medium was changed routinely in the presence of puromycin, and the cells were passaged at least twice before an experiment.

siRNA knockdown in myoblasts. Control myoblasts were seeded into 6-well plates and transfected with 100 nM control siRNA D-001810-10-05 (Horizon) *or* siRNA against Tango2 *L*-016397-02-0005 (Horizon), with Dharmafect transfection reagent (T-2001-01 Horizon, 5 uL/well).

Gene expression analysis in cells. Total RNA was isolated from skeletal muscle using NucleoSpin RNAXS kit (Macherey-Nagel). Single-stranded cDNA was synthesized from 1 µg of total RNA using the High Capacity RNA-to-cDNA Kit (Applied biosystems) after depleting genomic DNA. The expression of *MAP1LC3B* gene in skeletal muscle was assessed by RT-qPCR using Power SYBR® Green PCR Master Mix and normalized against *β-actin*. Primers are the followings: Forward 5' GATGTCCGACTTATTCGAGAGC 3', Reverse 5' TTGAGCTGTAAGCGCCTTCTA 3'. Reactions were performed in triplicate on an Azure Cielo Real-Time PCR machine (Azure Biosystem). The RQ value was equal to 2ΔΔct where ΔΔct is calculated by (Ct target- Ct β-actin) test sample - (Ct target- Ct β-actin) calibrator sample. Each value was derived from three technical replicates.

Western Blotting. Myoblasts or fibroblasts were lysed in RIPA buffer with protease inhibitors for 10 minutes on ice, prior to sonication (5 pulses, 5 seconds), and further 10 minutes on ice. Post-nuclear supernatants were quantified by BCA before loading equal amounts of protein per lane onto NuPage 4-20% Bis-Tris gels (ThermoScientific). Dry transfer onto PVDF membranes was done with the iBlot2 device according to the manufacturer's instructions (ThermoScientific). Primary antibodies anti-LC3-B (clone 4E12, MBL International, 1:1000), FLAG (Sigma 1:1000), TANGO2 (Proteintech 27 846-1-AP 1:500) and anti-β-actin (sc-81178, Santa Cruz Biotechnology, 1:1000) were detected by appropriate HRP-conjugated secondary antibody followed by ECL detection. To guarantee that the blots were measured in the linear range of exposure, all the blots were quantified at the maximal exposure level below saturation using ImageLab software (BioRad).

Confocal microscopy. Cells seeded onto glass cover slips were fixed with 2% paraformaldehyde, quenched with 300 mM glycine, and permeabilized using 0.2% saponin and 0.2% BSA in PBS. Primary antibodies were diluted in permeabilization buffer (LC3B 1:100, TOM20 (Santa-Cruz rabbit ref, FLAG 1:300), and secondary antibodies to 1:300. Nuclei were stained with DAPI (100 ng/ml). Image acquisitions were performed with a 63× oil immersion objective (NA 1.4) through a laser scanning confocal microscope (TCS SP8-3X STED; Leica Microsystems). Images were processed with FIJI. Colocalization analysis was performed with JACoP from ImageJ, throughout the entire volume of each cell, unless otherwise specified. Data are reported as the Mander's coefficient.

Zebrafish Maintenance. Adult and larval zebrafish (*Danio rerio*) were maintained at Imagine Institute (Paris) facility and bred according to the National and European Guidelines for Animal Welfare. Experiments were performed on wild type and transgenic zebrafish larvae from AB strains. Zebrafish were raised in embryo medium: 0,6 g/L aquarium salt (Instant Ocean, Blacksburg, VA) in reverse osmosis water 0,01 mg/L methylene blue. Experimental procedures were approved by the National and Institutional Ethical Committees. Zebrafish were staged in terms of hours post fertilization (hpf) based on morphological criteria and manually dechorionated using fine forceps at 24 hpf. All the experiments were conducted on morphologically normal zebrafish larvae.

Microinjections. Morpholino antisense oligonucleotides (amo; GeneTools, Philomath, USA) were used to specifically knockdown the expression of *tango2* zebrafish orthologue. The AMOs were designed to bind to the ATG (amo-1) or to a splicing region in exon3 (amo-2). The sequences of amo-1 and amo-2 are respectively: 5'-ACTTCAAGAAGATGATGCACATGAG-3' and 5'-ATAAGGATGATATTTACCGCTGAGG-3'. Control morpholino, not binding anywhere in the zebrafish genome, has the following sequence 5'-CCTCTTACCTCAGTTACAATTTATA-3'. The

GFP-LC3-RFP-LC3ΔG autophagy probe [25] was injected at a final concentration of 120 ng/μL along with the amo. All the microinjections were carried out at one cell stage.

Gene expression analysis in zebrafish. Total RNA was isolated from injected fish using TRIzol Reagent (Sigma) according to the manufacturer's protocol. First-strand cDNAs were obtained by reverse transcription of 1 µg of total RNA using the High-Capacity cDNA Reverse Transcription Kit (Roche), according to the manufacturer's instructions. Quantitative PCR amplification was performed with SyBer2X Gene Expression Assays using the following primers; (Fw) 5' TCTTGAAGTTCGACCCTCGGC 3' and (Rv) 5' CAAAAAACCTCTCCCCTGGGC 3'. Data were analyzed by transforming raw Ct values into relative quantification data using the delta Ct method. To assess the efficiency of tango2-AMO^{spE3} on tango2 exon 3 splicing, the same primers were used (the reverse primer targets exons 4 and 5). The PCR product was loaded on a 1% agarose gel.

Zebrafish locomotor analysis. Locomotor behavior of 50 hpf zebrafish larvae were assessed using the Touched-Evoked Escape Response (TEER) test. Briefly, zebrafish were touched on the tail with a tip and the escape response were recorded using a Grasshopper 2 camera (Point Grey Research, Canada) at 30 frames per second. Travelled distance was quantified frame per frame for each embryo using the video tracking plugin of FIJI 1.83 software (open source). For drugs treatment experiments, 30 hpf zebrafish embryos were raised in embryo medium containing 25 μM calpeptin, 0,5 μM or 1 μM atorvastatin dissolved in DMSO, and locomotor phenotype was assessed at 50 hpf as described above.

Autophagy analysis in zebrafish. To monitor autophagy flux in zebrafish, we co-injected the GFP-LC3-RFP-LC3ΔG probe developed by Mizushima's laboratory [26] with tango2-MO^{atg} zebrafish or tango2-MO^{spE3} zebrafish. Dechorionated 30 hpf zebrafish were dissociated in EDTA-trypsin 0,25% at 28°C and by trituration. Digestion was stopped with 10% fetal calf serum and suspended cells were strained with a 40 μM strainer. Cells were then centrifuged (5 min at 3000 rpm, 4°C),

washed and resuspended with cold HBSS, twice. As a proof of principle, we treated dissociated cells from control-MO condition with 50 nM bafilomycin A1 for 1 hour. Autophagy was activated in dissociated cells with 25 uM calpeptin for 1 hour. The proportions of GFP-positive cells and of RFP-positive cells were quantified by flow cytometry, as previously established [26] using a MACSQuant® Analyzer 10 Flow cytometer (Miltenyi Biotec, Germany). Dissociated cells from 30 hpf non injected zebrafish were used as a negative control for fluorescence and compensation was made with cells from 30 hpf dissociated zebrafish expressing GFP or RFP fluorescence only. Data were processed using FlowJoTM 10 (BD, USA).

Beta oxidation flux. Beta oxidation flux was measured in whole blood by a method adapted from Dessein et al [21]. Briefly, deuterated acylcarnitine produced after incubation of whole blood with carnitine and deuterated palmitate ([16-$^2H_3$, 15-$^2H_2$, 14-$^2H_2$, 13-$^2H_2$]-palmitate) were measured by LC-MS/MS.

Statistical analysis. Data were plotted and analysed using Prism (GraphPad, USA). Statistical details are indicated in the legends.

Acknowledgements

The authors thank the zebrafish platform and the cell-imaging platform, for technical assistance in confocal imaging acquisition and analysis; Etienne Morel, Perrine Renard, for insightful discussions. Lentiviruses were produced by the platform Structure Fédérative de Recherche Necker Vecteurs viraux et transfert de genes (Structure Féderative de Recherche Nêcker-Université Paris Descartes, S Fabrega). This work was supported by grants from Fondation Lejeune 2017 to PdL, Agence Nationale de la Recherche to PdL and PvE (ANR – AAPG 2018 CE17 MetabInf), the Association Française contre les Myopathies to PdL, SM, HdC and EK (AFM 2016 – 2018 n°19773; AFM 2022 – 2025 n°24269), Tango2 Research Foundation 2020 to PdL,

SM, HdC and EK, Prix Necker 2017 to PdL, Prix Sauver la vie Université Paris Cité 2020 to PdL, and patient associations (No Myolyse, Des ailes pour L, Nos Anges, OPPH, de Miniac en attente, Hyperinsulinisme, Noa Luû). SM was supported by a funding from the ANR – AAPG 2018 CE17 MetabInf.

Disclosure statement

The authors have no conflict of interest.

References

1. Lalani SR, Liu P, Rosenfeld JA, Watkin LB, Chiang T, Leduc MS, et al. Recurrent Muscle Weakness with Rhabdomyolysis, Metabolic Crises, and Cardiac Arrhythmia Due to Bi-allelic TANGO2 Mutations. Am J Hum Genet 2016; 98:347-57.
2. Kremer LS, Distelmaier F, Alhaddad B, Hempel M, Iuso A, Kupper C, et al. Bi-allelic Truncating Mutations in TANGO2 Cause Infancy-Onset Recurrent Metabolic Crises with Encephalocardiomyopathy. Am J Hum Genet 2016; 98:358-62.
3. Cervellin G, Comelli I, Lippi G. Rhabdomyolysis: historical background, clinical, diagnostic and therapeutic features. Clin Chem Lab Med 2010; 48:749-56.
4. Torres PA, Helmstetter JA, Kaye AM, Kaye AD. Rhabdomyolysis: pathogenesis, diagnosis, and treatment. Ochsner J 2015; 15:58-69.
5. Berat CM, Montealegre S, Wiedemann A, Nuzum MLC, Blondel A, Debruge H, et al. Clinical and biological characterization of 20 patients with TANGO2 deficiency indicates novel triggers of metabolic crises and no primary energetic defect. J Inherit Metab Dis 2020.
6. Dines JN, Golden-Grant K, LaCroix A, Muir AM, Cintron DL, McWalter K, et al. TANGO2: expanding the clinical phenotype and spectrum of pathogenic variants. Genet Med 2019; 21:601-7.
7. Jennions E, Hedberg-Oldfors C, Berglund AK, Kollberg G, Tornhage CJ, Eklund EA, et al. TANGO2 deficiency as a cause of neurodevelopmental delay with indirect effects on mitochondrial energy metabolism. J Inherit Metab Dis 2019; 42:898-908.
8. Meisner JK, Ames EG, Ahmad A, Si MS, Schumacher KR, Lim HM, et al. Heart Transplantation for TANGO2- Related Metabolic Encephalopathy and Arrhythmia (TRMEA) Syndrome Associated Cardiomyopathy. Circ Genom Precis Med 2020.
9. Mingirulli N, Pyle A, Hathazi D, Alston CL, Kohlschmidt N, O'Grady G, et al. Clinical presentation and proteomic signature of patients with TANGO2 mutations. J Inherit Metab Dis 2020; 43:297-308.
10. Scuotto F, Silva Jardim MF, Piazzon FB, Marcos de Moraes Albertini C, Assad RS, Fenelon G, et al. Electrical storm treated successfully in a patient with TANGO2 gene mutation and long QT syndrome: A case report. HeartRhythm Case Rep 2020; 6:256-60.
11. Miyake CY, Lay EJ, Soler-Alfonso C, Glinton KE, Houck K, Tosur M, et al. Natural History of TANGO2 Deficiency Disorder: Baseline Assessment of 73 Patients. Genet Med 2022.
12. Yokoi K, Nakajima Y, Takahashi Y, Hamajima T, Tajima G, Saito K, et al. Transport and Golgi organization 2 deficiency with a prominent elevation of C14:1 during a metabolic crisis: A case report. JIMD Rep 2023; 64:3-9.
13. Asadi P, Milev MP, Saint-Dic D, Gamberi C, Sacher M. Vitamin B5, a coenzyme A precursor, rescues TANGO2 deficiency disease-associated defects in Drosophila and human cells. J Inherit Metab Dis 2022.
14. Milev MP, Saint-Dic D, Zardoui K, Klopstock T, Law C, Distelmaier F, et al. The phenotype associated with variants in TANGO2 may be explained by a dual role of the protein in ER-to-Golgi transport and at the mitochondria. J Inherit Metab Dis 2020.
15. Casey J, Kim ES, Tao BS, Mansur A, Wallace ED, Gupta VA. Glycerolipid defects in skeletal muscle contribute to rhabdomyolysis in Tango2 deficiency
bioRxiv 2022.11.12.516274; doi: https://doi.org/10.1101/2022.11.12.516274.
16. Sun F, Zhao Z, Willoughby MM, Shen S, Zhou Y, Shao Y, et al. HRG-9 homologues regulate haem trafficking from haem-enriched compartments. Nature 2022; 610:768-74.
17. Heiman P, Mohsen AW, Karunanidhi A, St Croix C, Watkins S, Koppes E, et al. Mitochondrial dysfunction associated with TANGO2 deficiency. Sci Rep 2022; 12:3045.

18. Maynard TM, Meechan DW, Dudevoir ML, Gopalakrishna D, Peters AZ, Heindel CC, et al. Mitochondrial localization and function of a subset of 22q11 deletion syndrome candidate genes. Mol Cell Neurosci 2008; 39:439-51.
19. Lujan A, Foresti O, Brouwers N, Farre AM, Vignoli A, Wojnacki J, Malhotra V. Defects in lipid homeostasis reflect the function of TANGO2 in Acyl-CoA metabolism.
bioRxiv 2022.11.05.515282; doi: https://doi.org/10.1101/2022.11.05.515282
20. Sandkuhler SE, Zhang L, Meisner JK, Ghaloul-Gonzalez L, Beach CM, Harris D, et al. B-complex vitamins for patients with TANGO2-deficiency disorder. J Inherit Metab Dis 2022.
21. Dessein AF, Fontaine M, Dobbelaere D, Mention-Mulliez K, Martin-Ponthieu A, Briand G, et al. Deuterated palmitate-driven acylcarnitine formation by whole-blood samples for a rapid diagnostic exploration of mitochondrial fatty acid oxidation disorders. Clin Chim Acta 2009; 406:23-6.
22. Gibbs EM, Horstick EJ, Dowling JJ. Swimming into prominence: the zebrafish as a valuable tool for studying human myopathies and muscular dystrophies. FEBS J 2013; 280:4187-97.
23. Li M, Hromowyk KJ, Amacher SL, Currie PD. Muscular dystrophy modeling in zebrafish. Methods Cell Biol 2017; 138:347-80.
24. Guyon JR, Steffen LS, Howell MH, Pusack TJ, Lawrence C, Kunkel LM. Modeling human muscle disease in zebrafish. Biochim Biophys Acta 2007; 1772:205-15.
25. Mathai BJ, Meijer AH, Simonsen A. Studying Autophagy in Zebrafish. Cells 2017; 6.
26. Kaizuka T, Morishita H, Hama Y, Tsukamoto S, Matsui T, Toyota Y, et al. An Autophagic Flux Probe that Releases an Internal Control. Mol Cell 2016; 64:835-49.
27. Moss JJ, Hammond CL, Lane JD. Zebrafish as a model to study autophagy and its role in skeletal development and disease. Histochem Cell Biol 2020; 154:549-64.
28. Kawahara G, Maeda H, Kikura-Hanajiri R, Yoshida KI, Hayashi YK. The psychoactive drug 25B-NBOMe recapitulates rhabdomyolysis in zebrafish larvae. Forensic Toxicol 2017; 35:369-75.
29. Pasha R, Moon TW. Coenzyme Q10 protects against statin-induced myotoxicity in zebrafish larvae (Danio rerio). Environ Toxicol Pharmacol 2017; 52:150-60.
30. Sztal TE, Ruparelia AA, Williams C, Bryson-Richardson RJ. Using Touch-evoked Response and Locomotion Assays to Assess Muscle Performance and Function in Zebrafish. J Vis Exp 2016.
31. Kiage J, Venkatanarayan A, Roth M, Elam M. Atorvastatin-associated rhabdomyolysis in a patient with a novel variant of the SLCO1B1 gene: A case report. J Clin Lipidol 2022; 16:23-7.
32. He C, Bartholomew CR, Zhou W, Klionsky DJ. Assaying autophagic activity in transgenic GFP-Lc3 and GFP-Gabarap zebrafish embryos. Autophagy 2009; 5:520-6.
33. Watchon M, Yuan KC, Mackovski N, Svahn AJ, Cole NJ, Goldsbury C, et al. Calpain Inhibition Is Protective in Machado-Joseph Disease Zebrafish Due to Induction of Autophagy. J Neurosci 2017; 37:7782-94.
34. Jokl EJ, Blanco G. Disrupted autophagy undermines skeletal muscle adaptation and integrity. Mamm Genome 2016; 27:525-37.
35. Masiero E, Agatea L, Mammucari C, Blaauw B, Loro E, Komatsu M, et al. Autophagy is required to maintain muscle mass. Cell Metab 2009; 10:507-15.
36. Masiero E, Sandri M. Autophagy inhibition induces atrophy and myopathy in adult skeletal muscles. Autophagy 2010; 6:307-9.
37. Castets P, Frank S, Sinnreich M, Ruegg MA. "Get the Balance Right": Pathological Significance of Autophagy Perturbation in Neuromuscular Disorders. J Neuromuscul Dis 2016; 3:127-55.
38. Grumati P, Coletto L, Sabatelli P, Cescon M, Angelin A, Bertaggia E, et al. Autophagy is defective in collagen VI muscular dystrophies, and its reactivation rescues myofiber degeneration. Nat Med 2010; 16:1313-20.
39. Xia Q, Huang X, Huang J, Zheng Y, March ME, Li J, et al. The Role of Autophagy in Skeletal Muscle Diseases. Front Physiol 2021; 12:638983.

40. Hamel Y, Mauvais FX, Madrange M, Renard P, Lebreton C, Nemazanyy I, et al. Compromised mitochondrial quality control triggers lipin1-related rhabdomyolysis. Cell Rep Med 2021; 2:100370.
41. Byrne S, Jansen L, JM UK-I, Siddiqui A, Lidov HG, Bodi I, et al. EPG5-related Vici syndrome: a paradigm of neurodevelopmental disorders with defective autophagy. Brain 2016; 139:765-81.
42. Suliman I, Batarfi A, Almohammadi H, Aljeraisi H, Alnaserallah H, Alghamdi A. Prevalence of Self-Reported Muscle Pain Among Statin Users From National Guard Hospital, Riyadh. Cureus 2022; 14:e23463.
43. Al-Habsi AA, Massarsky A, Moon TW. Exposure to gemfibrozil and atorvastatin affects cholesterol metabolism and steroid production in zebrafish (Danio rerio). Comp Biochem Physiol B Biochem Mol Biol 2016; 199:87-96.
44. Li L, Tong M, Fu Y, Chen F, Zhang S, Chen H, et al. Lipids and membrane-associated proteins in autophagy. Protein Cell 2021; 12:520-44.
45. Zhang P, Verity MA, Reue K. Lipin-1 Regulates Autophagy Clearance and Intersects with Statin Drug Effects in Skeletal Muscle. Cell Metab 2014.
46. Noda T, Matsunaga K, Taguchi-Atarashi N, Yoshimori T. Regulation of membrane biogenesis in autophagy via PI3P dynamics. Semin Cell Dev Biol 2010; 21:671-6.
47. Weiyi Xu, Yingqiong Cao, Lorren Cantú, Eleni Nasiotis, Seema R. Lalani, Christina Y. Miyake, Lilei Zhang. TANGO2 deficient iPSC-differentiated cardiomyocyte and dermal fibroblasts have normal mitochondrial OXPHOS function. doi: https://doi.org/10.1101/2022.06.27.497853.

Tables

Table 1. Beta-oxydation Flux in whole blood of TANGO2 patients compared to controls

	C2-D3 (nmol/ G leucocytes/ 6 hours)	C4-D7 (nmol/ G leucocytes/ 6 hours)	C6-D9 (nmol/ G leucocytes/ 6 hours)	C8-D9 (nmol/ G leucocytes/ 6 hours)	C10-D9 (nmol/ G leucocytes/ 6 hours)	C12-D9 (nmol/ G leucocytes/ 6 hours)	C14-D9 (nmol/ G leucocytes/ 6 hours)	C14-OH-D9 (nmol/ G leucocytes/ 6 hours)	C16-D9 (nmol/ G leucocytes/ 6 hours)	C16-OH-D9 (nmol/ G leucocytes/ 6 hours)
Controls										
Median	56,9	15,9	96,7	3,6	43,0	85,1	21,3	4,5	1027,7	28,9
5th PC	19,4	5,9	39,3	1,2	12,2	32,8	9,3	0,9	465,2	0,0
95th PC	119,0	43,2	221,4	12,6	143,0	208,0	48,3	17,1	1961,3	65,4
TANGO2 patients										
Patient 1	116,14	21,95	78,66	3,35	53,21	205,44	18,47	3,90	716,21	18,31
Patient 2	83,97	19,90	170,08	4,51	86,16	217,01	30,29	16,39	690,93	48,75
Patient 3	25,88	15,48	117,25	8,38	38,18	87,63	45,33	3,10	2205,93	25,68

Figures legends

Figure 1. Autophagy is defective in *TANGO2* KO myoblasts.

A. Control and patient's myoblasts were cultured in Growth Medium (GM) or starved in EBSS for the indicated time points. Representative gels showing LC3-II reduction in three patients against a control. Baf=bafilomycin A1. **B** Quantification LC3-II at each time point upon starvation. Data are shown as the absolute values of the band intensity paired between control and patient on each individual experiment. n=3 controls, n=3 patients, with at least two technical replicates per patient. *p<0.05, **p<0.01, ***p<0.001 from paired Student t-test. **C.** Control myoblasts were transfected with siRNA oligonucleotide control or against tango2, and four days after transfection, cells were treated as in **A**. Gel represents three independent experiments with similar results. **D.** Expression of MAP1LC3B upon starvation (EBSS) in patient's primary myoblasts relative to controls. Data are presented as mean + SEM for three independent experiments. n=3 controls, n=3 patients. *p<0.05 from paired Student t-test. **E.** Fibroblasts from patients 1 and 2 were used in a similar experiment as on **A**, compared to control fibroblasts. Quantification of LC3-II protein levels represented as mean + SEM of N=3 independent experiments after 2h30 and 5h starvation. **F.** Patient 1 myoblasts' were transduced with the indicated viruses, incubated for 2h in EBSS, fixed, and stained against FLAG (TANGO2, green) and LC3 (red). Data represent two independent experiments per virus. Scale bar= 20 µm.

Figure 2. *Tango2* knockdown induces a RM-like phenotype in zebrafish due to autophagy defects.

A. Expression of tango2 zebrafish orthologue at 1 and 2 dpf embryogenic stages in zebrafish. Data are shown as mean + SEM. **B.** Representative pictures of 50 hpf whole zebrafish showing no defect on global morphology. **C**,**D** TEER results**. (C)** Representative swimming trajectories of

zebrafish individuals and **(D)** quantification of average swimming distance, reflecting impaired locomotor abilities of 50 hpf zebrafish from tango2-MO^{spE3} condition. Each dot represents one embryo. Data are shown as mean +/- SEM. ***p<0,001 and *ns* non-significant from Kruskal-Wallis and Dunn's multiple comparisons test. N=5. **E.** PCR strategy and representative gel electrophoresis of amplification products from 24 and 50 hpf zebrafish showing aberrant splicing products in tango2-MO^{spE3} zebrafish at both stages. **F.** Effects of 0,5 and 1 μM atorvastatin (ATV) treatments on zebrafish swimming properties as quantified by average swimming distance parameter by TEER test. Data are shown as mean + SEM. **p<0,01; ***p<0,001; ****p<0,0001 from 2-way ANOVA and Tukey's multiple comparison test. N=3. **G.** Monitoring of autophagy flux using the GFP-LC3-RFP-LC3Δ fluorescent probe. Autophagy index as quantified by GFP/RFP ratio by flow cytometry analysis of 30 hpf dissociated zebrafish, showing reduced autophagy flux (increased autophagy index) in tango2-MO^{spE3} zebrafish cells. Dissociated cells from control-MO zebrafish were treated with 50 nM bafilomycin as a positive control of decreased degradative efficiency of GFP-positive autophagosomes. Data are shown as mean + SEM. **p<0,01 from Kruskal-Wallis and Dunn's test. N=8.

Figure 3. Calpeptin ameliorates TANGO2 disease features in zebrafish and in primary myoblasts.

A. Average swimming distance from TEER test showing the beneficial effect of 25 μM calpeptin treatment on RM-like features of 50 hpf zebrafish. Data are shown as mean + SEM. *p<0,05; **p<0,01 and *ns* non-significant from 2-way ANOVA and Tukey's test. N=4. **B.** Autophagy index of 30 hpf zebrafish dissociated cells treated with 25 μM calpeptin, showing that calpeptin restores autophagy efficiency of tango2-MO^{spE3} zebrafish. 50 nM bafilomycin was used as a positive control of decreased degradative efficiency of GFP-positive autophagosomes. Data are shown as mean + SEM. *p<0,05; **p<0,01 from 2-way ANOVA and Tukey's test. N=6. **C**,**D** Western Blot

results of control and TANGO2 patients primary myoblasts cultured in growth medium (GM) or starved in EBSS, treated or not with 25 μM calpeptin. **(C)** Representative LC3 immunoblots from a single experiment out of N=4 independent experiments with similar results. '*ns* non-significant **(D)** LC3-II protein levels paired between control and patient on each individual experiment, showing that calpeptin treatment improves LC3-II levels in control and TANGO2 primary myoblasts. *$p<0.05$ and *ns* non-significant, from 2-way ANOVA and paired post-hoc Student t-tests.

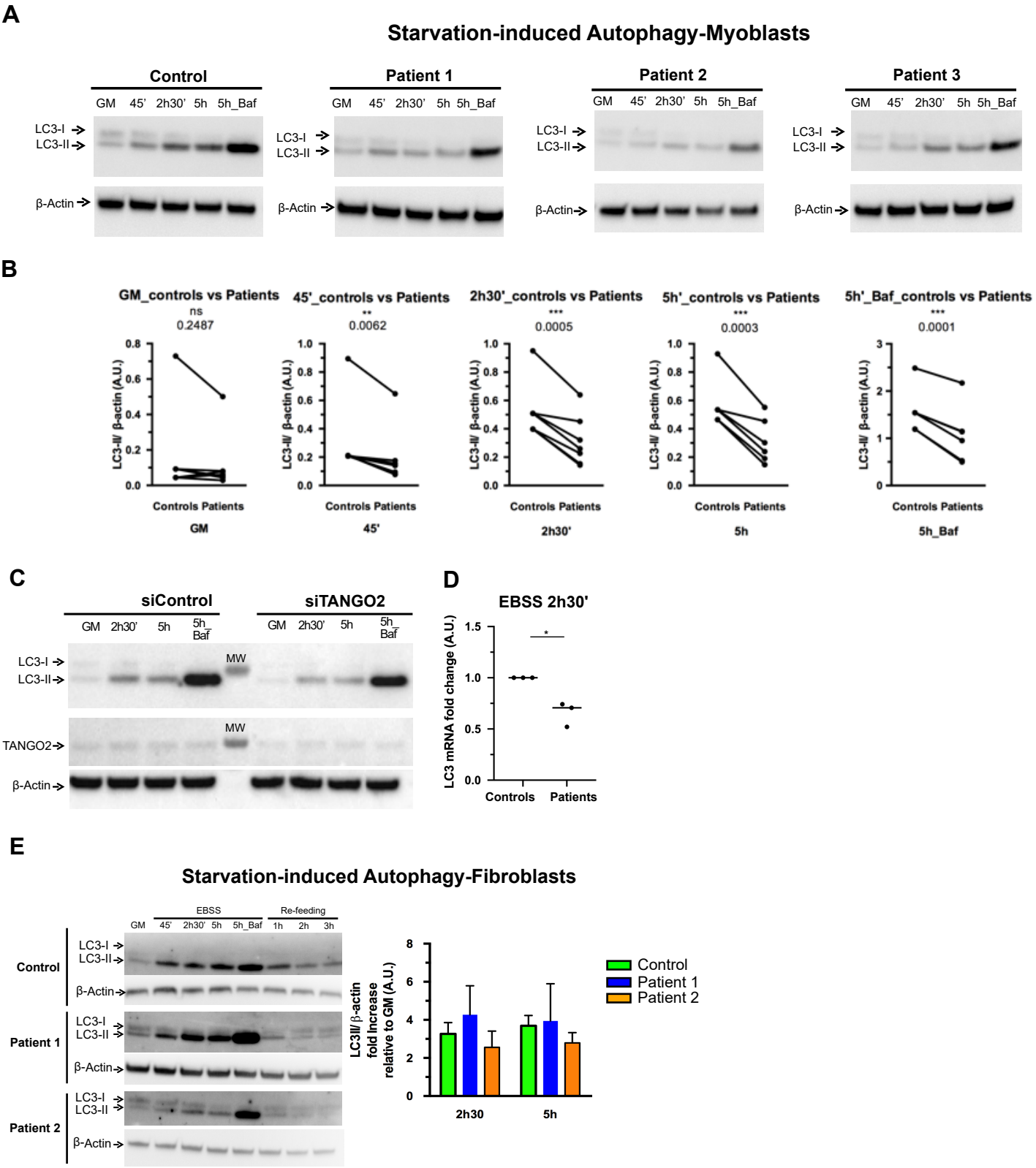
A
Starvation-induced Autophagy-Myoblasts
Control
Patient 1
Patient 2
Patient 3
GM 45' 2h30' 5h 5h_Baf
LC3-I
LC3-II
β-Actin
B
GM_controls vs Patients
ns
0.2487
45'_controls vs Patients
**
0.0062
2h30'_controls vs Patients
***
0.0005
5h'_controls vs Patients
***
0.0003
5h'_Baf_controls vs Patients
***
0.0001
LC3-II/ β-actin (A.U.)
Controls Patients
GM
45'
2h30'
5h
5h_Baf
C
siControl
siTANGO2
GM 2h30' 5h 5h_Baf
MW
TANGO2
D
EBSS 2h30'
LC3 mRNA fold change (A.U.)
Controls
Patients
E
Starvation-induced Autophagy-Fibroblasts
EBSS
Re-feeding
GM 45' 2h30' 5h 5h_Baf 1h 2h 3h
Control
Patient 1
Patient 2
LC3II/ β-actin fold Increase relative to GM (A.U.)
2h30
5h
Control
Patient 1
Patient 2
F
FLAG+LC3 EBSS 2h-Myoblasts
T2 WT C-ter FLAG
N-ter FLAG T2 WT
T2 G2R C-ter FLAG
N-ter FLAG T2 G2R

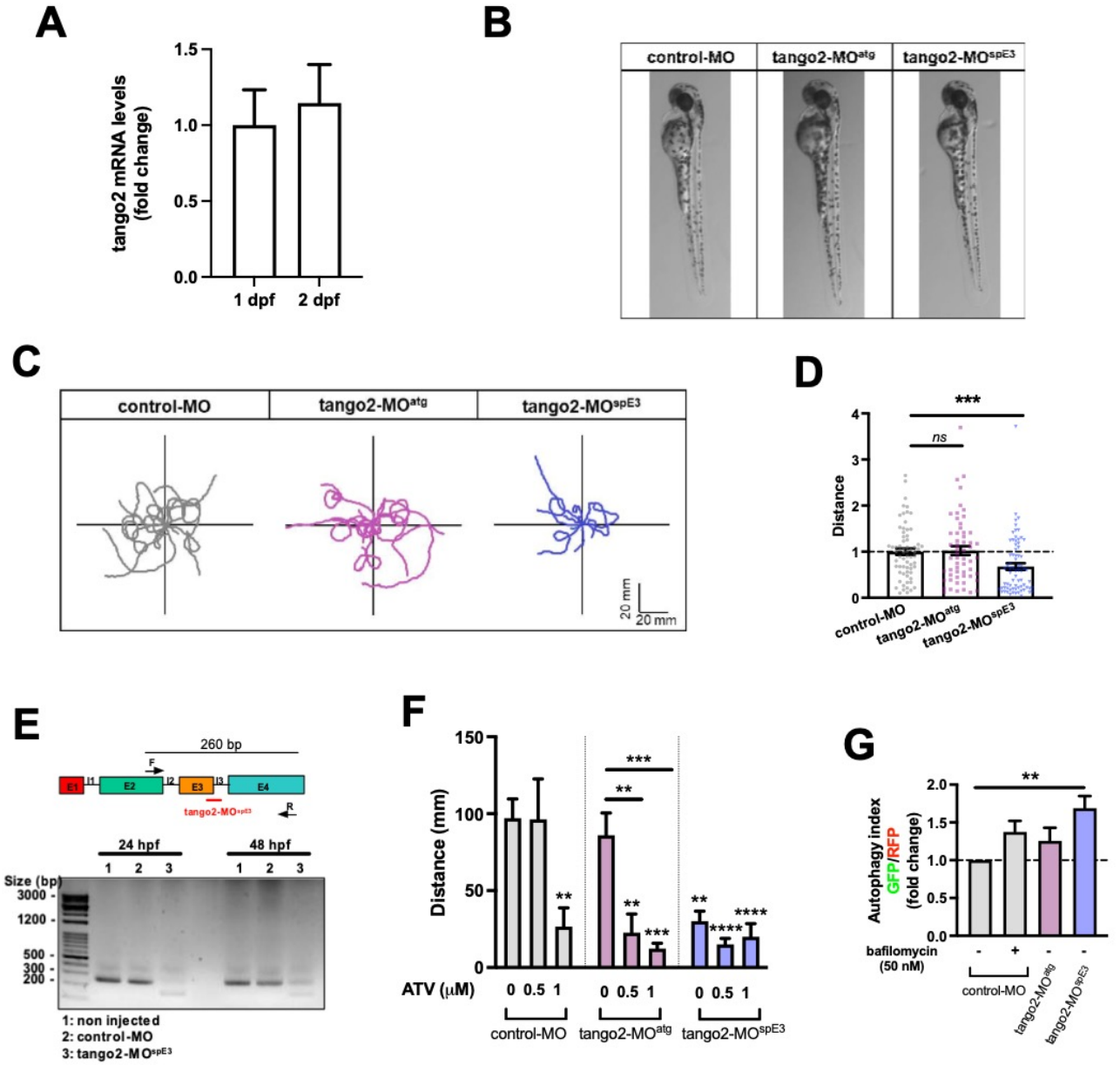
A
tango2 mRNA levels (fold change)
1.5
1.0
0.5
0.0
1 dpf
2 dpf
B
control-MO
tango2-MO^atg
tango2-MO^spE3
C
control-MO
tango2-MO^atg
tango2-MO^spE3
20 mm
20 mm
D
Distance
***
ns
control-MO
tango2-MO^atg
tango2-MO^spE3
E
260 bp
E1
I1
E2
I2
E3
I3
E4
F
R
tango2-MO^spE3
24 hpf
48 hpf
1 2 3
1 2 3
Size (bp)
3000
1200
500
300
200
1: non injected
2: control-MO
3: tango2-MO^spE3
F
Distance (mm)
150
100
50
0
***
**
**
***
**
****
****
ATV (μM)
0 0.5 1
0 0.5 1
0 0.5 1
control-MO
tango2-MO^atg
tango2-MO^spE3
G
Autophagy index GFP/RFP (fold change)
2.0
1.5
1.0
0.5
0.0
**
bafilomycin (50 nM)
- + - -
control-MO
tango2-MO^atg
tango2-MO^spE3

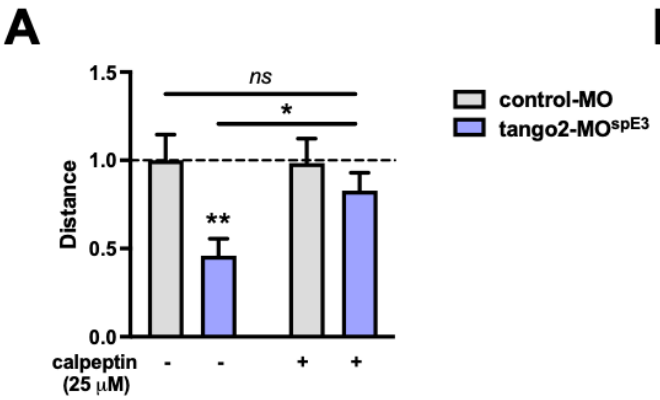
A
ns
*
**
Distance
1.5
1.0
0.5
0.0
calpeptin (25 μM)
- - + +
control-MO
tango2-MOspE3

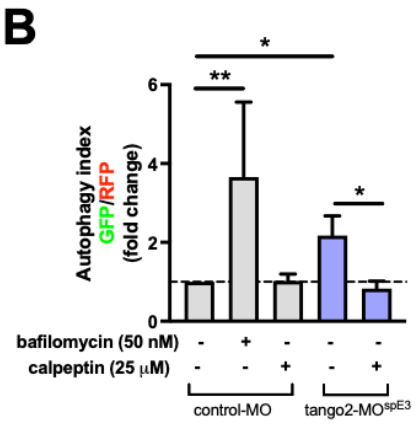
B
*
**
*
Autophagy index GFP/RFP (fold change)
6
4
2
0
bafilomycin (50 nM) - + - - -
calpeptin (25 μM) - - + - +
control-MO
tango2-MOspE3

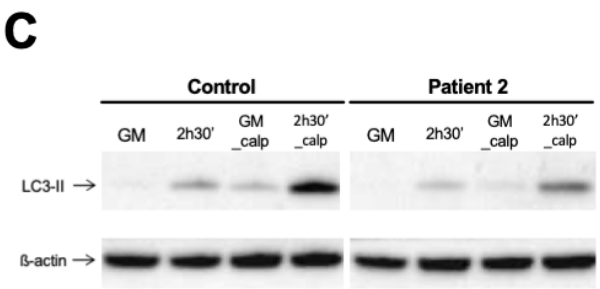
C
Control
Patient 2
GM
2h30'
GM _calp
2h30' _calp
GM
2h30'
GM _calp
2h30' _calp
LC3-II
ß-actin

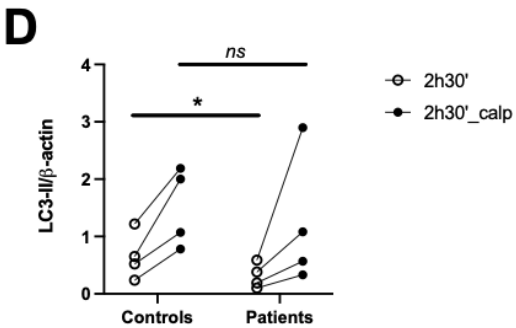
D
ns
*
LC3-II/β-actin
4
3
2
1
0
Controls
Patients
2h30'
2h30'_calp